RSC Advances

1   Integrated Analysis of Serum and Intact Muscle Metabonomics
2   Identify Metabolic Profiles of Cancer Cachexia in a Dynamic
3   Mouse Model

4

5

6

7   Yang QuanJun[1,#], Yang GenJin[2#], Wan LiLi[1], Huo Yan[1], Han YongLong[1], Lu Jin[1], Li

8   Jie[1],Huang JinLu[1],Guo Cheng[1*]

9

10   1, Department of Pharmacy, Shanghai Jiao Tong University Affiliated Sixth People's

11   Hospital, Shanghai 200233, P. R. China

12   2, School of Pharmacy, Second Military Medical University, Shanghai 200433, P. R. China

13

14   [#] Contributed equally for the manuscript

15   **Corresponding author:**

16   Guo Cheng. Shanghai Jiao Tong University Affiliated Sixth People's Hospital, No. 600,

17   Road Yishan, Shanghai, 200233, China. Phone # +86 21 24058098; E-mail:

18   guopharm@126.com.

19

1   **Abstract**

2   Cancer cachexia is a multifactorial metabolic syndrome characterized by a severe loss of body

3   weight and lean body mass. Metabolic dysfunction is the primary hallmark of muscle atrophy.

4   Herein, we studied dynamic metabolic profiles in serum and intact muscle. High-resolution

5   magic angle spinning was employed to intact gastrocnemius muscle analysis and a dynamic

6   metabolic model was established using C26 colon carcinoma-bearing mice from procachexia

7   to the refractory cachexia period. When integrated analysis of the 13 metabolites from intact

8   muscle gastrocnemius and 43 metabolites from serum, five distinguishable metabolic features

9   were identified, including low blood glucose, elevated ketone bodies, decreased branched -

10 chain amino acids, increased neutral amino acids, and high 3-methylhistidine and creatine.

11 The metabolic hubs reveal potential biomarkers for the early detection of cachexia and

12 indicate the underlying metabolic pathway reprogramming of muscle atrophy.

13

14 Keywords: Cancer cachexia; Muscle atrophy; Metabonomics; NMR; Branched-chain amino

15 acid

1   **1.Introduction**

2   Cachexia is a multifactorial metabolic syndrome that occurs in up to 80% of advanced cancer

3   patients and contributes to approximately 30% of cancer mortality [1, 2]. It is associated with

4   reduction in quality of life, the response to therapeutic modalities and treatment tolerance [3].

5   Lean body mass depletion is the most paradigmatic contribution to the severe body weight

6   loss observed in cachexia, and it indicates a poor prognosis [4]. Recent developments have shed

7   light on the central role of maintaining skeletal muscle mass in the prevention and treatment

8   of cachexia [5]. Research has shown that the prevention of muscle wasting not only reverses the

9   symptoms of cachexia but also dramatically prolongs survival, without influencing the level

10   of fat loss or tumor growth [6]. The loss of skeletal muscle cannot be reversed by appetite

11   stimulants or nutritional support [7, 8], and there is no pharmacological treatment that can

12   sufficiently prevent the ongoing skeletal muscle wasting. Therefore, the regulatory

13   mechanisms underlying skeletal muscle metabolism are a topic of great interest.

14   The depletion of skeletal muscle in cancer cachexia is due to muscle fiber atrophy [9], which

15   results from increased protein catabolism (hypercatabolism) or decreased protein synthesis

16   (hypoanabolism) [10]. The presence of hypoanabolism suggests a shortage of the essential

17   substrates for the net accumulation of muscle protein and the failure of the normal stimuli for

18   muscle protein synthesis [11],whereas hypercatabolism potentially involves the excessive

19   production of catabolic stimuli and activation of the ubiquitin-proteasome pathway. The

20   mechanisms of hypoanabolism and hypercatabolism suggest possible metabolic hubs and

21   altered pathways for skeletal muscle research [12]. However, the underlying mechanisms that

22   trigger and exacerbate cachexia-associated metabolic disorders remain elusive.

23   Although previous studies conducted in animal models and in humans have found that blood

24   hyperlipidemia, hypoglycemia and decreasing levels of branched-chain amino acids (BCAAs)

25   are associated with cancer cachexia [13-15], the specificity of these markers has been challenged,

26   and the distinct metabolites in the skeletal muscle remain unknown. Moreover, metabolic

27   dysfunction occurs before the symptoms of muscle atrophy, and the regulation of metabolism

28   underlie the potential etiology and consequences of the subsequent weight loss. However,

29   direct study of the skeletal muscles is unachievable with the currently available biochemical

30   examinations and magnetic resonance imaging. However, integrated analysis of the skeletal

31   muscle and serum could reveal biomarkers for the diagnosis of muscle atrophy and cancer

32   cachexia. Metabolite changes in the skeletal muscle are associated with physiological

33   dysfunction; therefore, the altered metabolites might reveal the mechanism underlying protein

34   catabolism and synthesis.

35   In the present study, an approach consisting of the integrated analysis of serum and intact

1   muscle metabonomics was employed to identify the early biomarkers of muscle atrophy and

2   to reveal the metabolic regulatory mechanism underlying cancer cachexia. The gastrocnemius

3   muscle was evaluated using high-resolution magic-angle spinning (HR-MAS) NMR

4   spectroscopy. To identify metabolic profiles that were not affected by the cancer, a dynamic

5   metabolic approach was employed by acquiring samples at continuous time points, from

6   non-cachexia to the refractory cachexia period, from C26 colon carcinoma-bearing mice. The

7   distinct metabolite hubs in the altered pathways not only could be used for the early detection

8   of cancer cachexia but could also reveal the potential metabolic mechanism underlying cancer

9   cachexia.

10   **2.Materials and methods**

11   **2.1 Murine model of cancer cachexia**

12   All of the procedures involving animals and their care in this study were approved by the

13   animal care committee of our institution, in accordance with the institutional requirements

14   and the Chinese government guidelines for animal experiments. Male BALB/c mice were

15   purchased from Shanghai SLAC Laboratory Animal Co., Ltd. (Shanghai, China). The mice

16   were maintained in pathogen-free conditions with a constant temperature ($24+2°C$) and

17   humidity (relative humidity of $55\pm15\%$) and a 12:12 dark-light cycle. There was free access

18   to water and identical standard food (when permitted) for all of the subjects.

19   The murine C26 colon carcinoma model for inducing cachexia was established as previously

20   described [16, 17]. Briefly, BALB/c mice were randomly divided into groups and were

21   subcutaneously injected with a suspension of 10^6 C26 cells in the left flank. The control mice

22   were treated with an equivalent volume of PBS.

23   **2.2 Experimental design**

24   Two studies were performed. The first study assessed the relevance of the cancer cachexia

25   model with the clinical features of body weight, muscle weight, and tumor size. Beginning the

26   day on which the mice were injected with the C26 adenocarcinoma cells, total body weight

27   and food intake were measured daily. Tumor length and width were measured using digital

28   calipers once the tumor was palpable, and in vivo tumor weight was calculated using the

29   following equation: $0.52\times length\times(width)^2$. Body weight was calculated as the total body

30   weight minus the tumor weight. A second study was performed to reveal the dynamic

31   metabolic profile of cancer cachexia. A total of eight groups were designed and every group

32   had six to eight mice. The body and muscles were measured as the first experiment. Moreover,

33   serum and the intact gastrocnemius muscle were acquired from the same mice following

34   euthanasia via the inhalation of carbon dioxide, which was performed at continuous time

35   points from procachexia to the refractory cachexia period. On every other day, from the ninth

4

1 day to the twenty-first day, blood was collected in tubes. The heart, epididymis adipose tissue,

2 gastrocnemius muscle and tibialis anterior muscle were dissected, weighed and quickly frozen

3 in liquid nitrogen. The mice were then skinned, and the tumors were removed to measure the

4 carcass body weight.

5 **2.3 Western blot analysis**

6 The gastrocnemius muscles from the model animals were homogenized and solubilized in

7 lysis buffer using a commercial kit (Beyotime Institute of Biotechnology, Jiangsu, China).

8 Briefly, 50 mg of tissue was extracted with lysis buffer (containing phenylmethanesulfonyl

9 fluoride) to obtain low molecular weight soluble protein. The precipitate was then extracted

10 with a hypertonic lysis buffer. After evaluating the protein content using a bicinchoninic acid

11 protein assay kit (Pierce, Rockford, USA), the protein was solubilized in loading buffer and

12 boiled at 95°C for 5 minutes. Equal amounts of the protein samples (20 mg) were loaded on a

13 10% SDS-polyacrylamide gel to separate the muscle ring finger-1 (MuRF1) protein and on an

14 8% SDS-polyacrylamide gel to isolate the myosin heavy chain (MHC) protein. Subsequently,

15 the proteins were electrophoretically separated and transferred onto PVDF membranes

16 (Millipore Corporation, Bedford, USA) for western blot analysis. The blots were then

17 incubated with the primary antibodies anti-MHC (ab51263, 1:1000 dilution, Abcam,

18 Cambridge, USA) and anti-MuRF1 (ab77577, 1:1000 dilution, Abcam, Cambridge, USA),

19 according to the manufacturer's specifications. The proteins were detected using a

20 peroxidase-conjugated secondary antibody (1:5000 dilution in Tris-buffered saline with

21 Tween-20) with a chemiluminescence system and ImageQuant software.

22 **2.4 ^{1}H-NMR spectroscopy of the serum**

23 The plasma samples were prepared for NMR analysis by mixing 200 μL of plasma with 400

24 μL of PBS (containing 10% v/v D_2O). All of the spectra were recorded using a Bruker Avance

25 II 600 NMR spectrometer operated at a 600.13-MHz 1H resonance frequency. To attenuate

26 the broad NMR signals from slowly tumbling molecules (such as proteins), a standard

27 Carr-Purcell-Meiboom-Gill (CPMG) pulse sequence was used to record the 1D spin-echo

28 spectra. A pre-saturation solvent was also employed to suppress the water peaks. Briefly, the

29 CPMG pre-saturation pulse sequence worked using the equation -RD-90°-(t-180°-t)$_n$ - ACQ,

30 where RD is the relaxation delay of 2 s; 90° and 180° represent the RF pulses that trip the

31 magnetization vector; t is the spin-echo delay of 400 μs; n represents the number of loops

32 (which was 80 in our experiment); and ACQ is the data acquisition period of 1.36 s [18]. In our

33 experiment, the data points were acquired using 128 transients, and the number of time

34 domain points was 32k.

35 **2.5 ^{1}H-MAS NMR spectra of the gastrocnemius muscle**

1 The intact gastrocnemius muscle tissue (approximately 10 mg of tissue) was also evaluated

2 using NMR spectra. To eliminate the line broadening resulting from the macroscopic

3 magnetic field in the homogeneities and the microscopic susceptibility differences in the

4 intact tissue samples, 4 mm HR-MAS 1H/13C probe (Bruker Biospin) was equipped into

5 Bruker Avance II 600 NMR spectrometer to obtain the HR-MAS NMR spectra. The samples

6 were rinsed with D_2O for about 10 minutes and immediately transfer into an MAS rotor using

7 tweezers. The measurements were obtained at constant 303k to reduce any metabolic

8 degradation. To remove the spectral-broadening effects due to the interaction of solids, such

9 as dipolar couplings and chemical shift anisotropy, the pulse sequence of 1D NOESY

10 (noesypr1d) was used with the relaxation delay (RD) -- $90°-t_1-90°-t_m-90°$ -acquired free

11 induction decay (FID). The RD represents a relaxation delay of 1.5 s for the selective

12 irradiation of water resonance. The $90°$ pulse length was 5.2 μs, and t_1 was fixed at 4 μs.

13 Following a mixing time (tm) of 150 ms, a second pulse was performed, and the saturation of

14 the water residual signal was achieved by irradiating during the recycle delay at a δ equal to

15 4.70 ppm. The data points were recorded using a 5 kHz spinning speed with 256 transient

16 acquisitions. The FIDs were multiplied by an exponential weighting factor corresponding to a

17 line broadening at 0.3 Hz. After the Fourier transformation, phase correction and baseline

18 correction were carefully performed using the TopSpin software package (Bruker Biospin,

19 Rheinstetten, Germany), version 3.0. The ^{1}H chemical shifts referred to the methyl doublet

20 signal of lactate (δ1.33).

21 **2.6 Data reduction of the NMR data**

22 The corrected NMR spectra, corresponding to the chemical shift range of δ 0.2-10.0, were

23 imported into AMIX 3.9.5 (Bruker Biospin, Rheinstetten, Germany), and all of the spectra

24 were reduced into integral regions of equal lengths of 0.005 ppm. Regions of δ 4.7-5.1 that

25 contained the resonance from residual water were set to zero. To reduce the concentration

26 differences between the samples, the data were normalized to the total spectral area (100%).

27 **2.7Metabonomics analysis**

28 The dataset was analyzed by pattern recognition methods using the software packages

29 Simca-P, version 11.5 (UmetricsAB, Umeå, Sweden), and MetaboAnalyst, version 2.0

30 (www.metaboanalyst.ca). The dataset was arranged with the samples as observations and the

31 peak areas of the chemical shifts as the response variables. Before multivariate statistics were

32 performed, the response variables were centered and scaled to Pareto variance. The base

33 weight was computed as 1/sqrt (standard deviation of the response variables). Moreover, to

34 make the skewed distributions more symmetric, log transformations were used for nonlinear

35 conversions of the data.

1   To explain the maximum variation between the samples, a principal component analysis (PCA)

2   bilinear decomposition method was used to view the clusters within the multivariate data.

3   Moreover, partial least squares-discriminant analysis (PLS-DA) was applied to explain the

4   maximum separation between the defined class samples in the data. Three parameters, R^2X,

5   R^2Y and Q^2, were used for the evaluation of the models. R^2X explains the cumulative

6   variation in the response variables, and R^2Y is the latent variable of the sum of squares of all

7   of the Xs and Ys. Q^2 reflects the cumulative cross-validated percentage of the total variation

8   that can be predicted by the current latent variables. High coefficient values of R^2Y and Q^2

9   represent good discrimination and predictive ability, respectively. The specific metabolites

10 between classes were interpreted using variable importance in the projection (VIP) and

11 correlation coefficients. The variables with a high VIP are considered to be statistically

12 significant; therefore, VIP statistics was applied for metabolic pathway analysis.

13 **2.8 Metabolite identification**

14 Based on the statistical results of the metabonomics analysis, the discriminating peaks were

15 prioritized for identification. The NMR signals were compared with reference spectra from

16 the HMDB database and with Chenomx NMR Suite metabonomics software (Chenomx, Inc.,

17 Alberta, Canada), based on the coupling constant and the splitting model. The signal

18 assignments were conducted out using the 2D J-resolved, COSY, and TOCSY spectra. The

19 overlaps or slight shifts in their positions were confirmed by re-recording the ^{1}H NMR spectra

20 of the serum after the addition of small quantities of the respective standard compounds.

21 **2.9 Metabolic pathway analysis**

22 To identify the most relevant metabolic pathways involved in cancer cachexia, metabolomic

23 pathway analysis was employed to perform the pathway enrichment analysis and pathway

24 topology analysis. The pathway enrichment analysis used GlobalTest and GlobalAncova to

25 analyze the concentration values with high sensitivity in order to identify subtle changes

26 involved in the same biological pathway. However, a relative betweenness centrality was used

27 for the metabolite importance measurement and the established global network topology

28 analysis for its ability to order the metabolic pathways according to their positions. Changes

29 in a more important node of the network triggered a more severe impact on the pathway than

30 changes that occurred in marginal or relatively isolated positions.

31 **2.10 Statistical methods**

32 The data are expressed as the means ± SDs. The calculated means were statistically analyzed

33 using Origin software, version 8.1 (OriginLab Corp., Northampton, MA, USA). The

34 differences between the two groups were analyzed using Student's two-sided t test, and

35 differences involving more than two groups were analyzed using one-way ANOVA, followed

1   by Tukey's post hoc test. The level of significance was set at $p<0.05$.

2   **3.Results**

3   **3.1 CT26 tumor induced cancer cachexia resulting in ongoing loss of body weight and**

4   **skeletal muscle in mice**

5   The growth of C26 colon carcinoma resulted in impaired body weight gain that was

6   associated with a progressive loss of skeletal muscle weight. On day 13 following tumor

7   implantation, the body weights of the mice differed from the control values by at least 5%,

8   which was statistically significant (Fig. 1). To explore the changes in body composition

9   associated with cancer cachexia, the mice were sacrificed, and the weights of the organs,

10   skeletal muscle, fat and the wet and dry carcass were determined. The lean body weight loss

11   is presented relative to the significant loss of skeletal muscle. In particular, the mass of the

12   gastrocnemius and tibialis anterior muscles decreased by more than 20% on day 13 and

13   reached approximately 45% on day 21. The ongoing loss of wet carcass weight was consistent

14   with that for dry carcass weight, and the correlation coefficient was 96.88% (Table 1). The

15   decreased dry carcass weight was mainly due to muscle wasting, and these results indicated

16   that the body weight loss was due to muscle atrophy in the murine cachexia model.

17   MHC expression was significantly decreased during the cachexia period (17 d and 21 d).

18   MHC is degraded by the ubiquitin-proteasome system, as suggested by the increase in the

19   muscle-specific E3 ubiquitin ligase MuRF1 from day 13, which has previously been

20   associated with decreased MHC content [19, 20]. The dynamic loss of muscle weight and

21   increase in MuRF1 indicated the progression of cancer cachexia over the duration of the

22   sampling.

23   **3.2 Disorders of serum metabolic profiling is a hallmark of cancer cachexia**

24   The typical ^{1}H NMR spectra of the serum demonstrated a unique metabolic profile along with

25   the metabolite assignments (Fig. 2). The spectra contained very high-intensity signals from

26   glucose, lactate, creatine, alanine and VLDL/LDL. Moreover, numerous signals from the

27   dynamic cachexia mouse model showed marked changes in the levels of the endogenous

28   metabolites compared with the control mice, including pyruvate, acetate, 2-oxoglutarate,

29   phenylalanine, glycine, leucine, valine, isoleucine, glutamine, choline, succinate, acetate,

30   carnitine, and citrate.

31   To illustrate the differences in the metabolic profiles, the NMR spectra dataset were subjected

32   to PCA. The score plot revealed distinct separation of the tumor-bearing model (G1-G7) from

33   the control mice (G8). Moreover, the samples from the procachexia group (G1-G2) clustered

34   together, and the samples from the later cachexia period (G5-G7) clustered in a different

1   region. Though the discrimination was visible, the cumulative R^2X was 0.433 and Q^2 was

2   0.278 with 4 principal components. Therefore, a supervised PLS analysis was also applied to

3   the data after Pareto scaling, and it showed well-separated clusters (Fig. 3). Three principal

4   components were gave and the cumulative R^2X, R^2Y and Q^2 was 0.663, 0.997, 0.925

5   respectively. The high values of R^2Y and Q^2(cum) represent good discrimination and

6   predictive ability. The G1 and G2 groups clustered closely to the control group, suggesting

7   that the homeostasis during the initial cancer cachexia period was similar to that of the control

8   group. The G5, G6 and G7 groups were clustered in other regions, indicating the typical

9   cancer cachexia metabolic profile. The datasets were analyzed using MetPA and showed

10 similar score-loading plots (Fig. S1 in the Supplementary Material). The significantly

11 different metabolites, as well as the *p* values of the dynamic model mice, were calculated

12 (Table S1 and Fig. S2 in the Supplementary Material). The relative intensity levels are

13 partially shown in Fig. 4, including the increased glutamate, 3-hydroxybutyrate, citrate,

14 isocitrate, malate, arginine, creatine, carnitine, taurine, TMAO, 3-methylhistidine, glycine,

15 and phenylalanine levels and decreased glucose, 2-oxoglutarate, succinate, ornithine, leucine

16 and valine levels.

17 **3.3 MAS NMR reveals the distinct metabolic features for skeletal muscle atrophy during**

18 **cachexia**

19 Because muscle atrophy is the primary factor contributing to body wasting in cachexia, an

20 analysis of the skeletal muscle metabolites could provide a direct clue for biomarker research.

21 Unlike the serum metabolic spectra, there was a low concentration of glucose, and the most

22 abundant metabolite was creatine, which was relatively low compared with the control group

23 and which increased from procachexia to cachexia (Fig. 5). The overall spectra revealed

24 endogenous metabolites without degradation or lysis. Subtle changes in specific metabolites

25 in the skeletal muscle were observed, including in taurine, 3-methylhistidine, creatine, inosine,

26 carnosine, and 3-hydroxybutyrate (Fig. 6). This finding showed that the MAS NMR spectra

27 could highlight the original perturbations of the endogenous metabolites in the controls and

28 the dynamic mouse model.

29 PCA revealed complete separation between the cachexia group and the control group in the

30 scores plot (Fig. S3 in the Supplementary Material). Five principal components were gave and

31 the R^2X was 0.822. Similar to the serum samples, the gastrocnemius muscles of the cachexia

32 mice showed a dynamic metabolic profile, whereas the procachexia group clustered closely to

33 the control group. To find the corresponding different metabolites, PLS-DA was employed

34 and two principal components were gave with R^2X, R^2Y and Q^2(cum), 0.605, 0.929, 0.881

35 respectively. The S-plot (Fig. S4 in the Supplementary Material) displayed compromised

36 insulin action and altered intermediate metabolism of the fats and amino acids. Based on

1   multiple tests, the dynamic changes included increased phenylalanine, 3-methylhistidine,

2   inosine, taurine, creatine, carnitine, glycine, 3-hydroxybutyrate, and lactate and decreased

3   leucine, valine, isoleucine, and glucose (Fig. 6 and Table S2 in the Supplementary Material).

4   In particular, changes in the muscle concentrations of select essential amino acids and their

5   derivatives, particularly the BCAAs, the sulfur amino acids and phenylalanine were apparent,

6   in addition to muscle atrophy, both of which often occurred before the onset of clinically

7   diagnosed cachexia.

8   **3.4 Integrated analysis of serum and intact muscle metabonomics revealed the five**

9   **distinguishable metabolic features of cancer cachexia**

10   MetPA presented 21 altered metabolic networks (Fig. 7), with a detailed score of impact and

11   -log(p) (Table S3 in the Supplementary Material). Valine, leucine and isoleucine biosynthesis

12   were the most impacted pathways, which were calculated using pathway topology analysis.

13   Three matched metabolites of valine, leucine, and isoleucine were gradually reduced, and the

14   difference was significant. Additionally, ketone body synthesis and degradation pathway were

15   enhanced, with a 0.60 impact factor. The ketone bodies were primarily metabolized from

16   lipids and emerged as a compensatory mechanism of glucose metabolism. The cachexia

17   syndrome resulted in the synthesis and release of ketone bodies into the blood, causing the

18   acetoacetate levels to rise gradually and inducing hypolipidemia during the later cachexia

19   period. The high ketone levels were toxic and prompted ketoacidosis, indicating ketone body

20   metabolism and pyruvate metabolism in cancer cachexia.

21   The cachexia pathways that stood out the most were phenylalanine biosynthesis. As an

22   aromatic amino acid, phenylalanine is primarily metabolized in the liver. The presence of

23   phenylalanine indicates impaired hepatic function and negative regulation of food intake,

24   corresponding to the biochemical parameters of transaminase from other reports [21-23].

25   Among the marked endogenous metabolite perturbations, pathway analysis further showed

26   subtle changes in taurine and hypotaurine metabolism, glycine, serine and threonine

27   metabolism, glycerolipid metabolism, glyoxylate and dicarboxylate metabolism, the citrate

28   cycle (TCA cycle), alanine, aspartate and glutamate metabolism, glycolysis and

29   gluconeogenesis, inositol phosphate metabolism, cysteine and methionine metabolism,

30   arginine and proline metabolism, and glycerophospholipid metabolism. Interestingly, the

31   metabolic intermediates of the amino acids, such as creatine, carnitine, taurine, TMAO and

32   3-methylhistidine, steadily increased during the ongoing progress of cancer cachexia. An

33   additional multigroup analysis of the compounds revealed that the gradual increases in the

34   intermediate metabolites occurred along with the accumulation of nitrogen and the

35   aggravation of muscle wasting.

1   Multivariate data analysis of serum and intact muscle metabonomics from continuous stages

2   in the murine cachexia model indicated that there were distinguishable profiles of serum and

3   muscle metabolites. However, similar differences appeared in the composition and

4   concentration of metabolite hubs. After the integrated analysis of the metabolic profiles

5   obtained from serum and intact muscle, the distinct metabolic characteristics included low

6   blood glucose, high ketone bodies, decreased BCAAs, increased phenylalanine and elevated

7   amino acid intermediates.

8

1   4. **Discussion**

2   Currently, dual-energy X-ray absorptiometry is considered to be the gold standard for

3   assessing muscle wasting; however, this method provides little chemical information and has

4   limited ability to detect early wasting of skeletal muscle [24]. In fact, metabolic disorder occurs

5   prior to the wasting observed in cachexia, and metabolites can be used for the early detection

6   of cancer cachexia [25, 26]. Previous metabolomic research into cancer cachexia was based on

7   NMR analysis of serum; however, the blood metabolites were not sufficient to provide

8   detailed functional data on the biochemistry of muscle wasting. Instead, intact muscle can

9   reveal tissue-specific metabolic processes, as well as allow for the integration of data

10   collected from multiple experiments. The major issue for the analysis of intact muscle is the

11   anisotropic electronic and magnetic interactions between the nuclei in intact biological tissues,

12   which cannot be completely averaged, resulting in broad lines in a conventional NMR

13   spectrum [27]. MAS based NMR spectra provided narrow lines and well-resolved samples, and

14   the intact muscle tissue could be analyzed nondestructively [28]. Thus, in our study, the

15   metabolic disorders of intact gastrocnemius muscle were analyzed with HR-MAS NMR

16   technology.

17   In the present study, we performed integrative metabolic profiling of the serum and intact

18   skeletal muscle tissue of mice with cachexia using ^{1}H-NMR-based metabonomics methods to

19   identify early biomarkers of muscle atrophy and cancer cachexia and to examine the

20   metabolic regulation of protein catabolism and synthesis. Forty-three distinguishing

21   metabolites were found to be altered significantly in the serum, and thirteen metabolites were

22   altered in the gastrocnemius muscle during the dynamic progression of cancer cachexia.

23   Although there have been metabolomic reports on the identification of serum and urine

24   biomarkers in cancer cachexia [13,14], the present study revealed the specifically altered

25   metabolites in intact skeletal muscle tissues in a dynamic manner.

26   Consistent with previous reports, decreased levels of glucose and increased levels of lactate

27   were observed in both the serum and intact gastrocnemius muscle. Tumor-bearing mice

28   require glucose at a faster rate than healthy animals. However, the glucose is metabolized and

29   enters the glycolytic pathway, leading to greater pyruvate formation. The majority of the

30   pyruvate is then disposed via non-oxidative pathways and is diverted into lactate and alanine,

31   rather than being oxidized via the citric acid cycle [29]. Excessive lactate production exacerbates

32   energy wasting and induces higher glucose uptake and utilization [30]. Reports have shown that

33   altered glucose metabolism is associated with whole-body protein turnover [23]. Skeletal muscle

34   is the primary target of glucose uptake, the disruption of glucose metabolism and its

35   intermediate metabolites bears some characteristics similar to tumor cell metabolism. Thus, its

1   specificity for the evaluation of muscle wasting was limited.

2   High ketone bodies were also observed in the blood and showed changing tendencies. The

3   increase in ketobodies in the gastrocnemius muscle can also be viewed as a characteristic of

4   muscle wasting. Although neither the ATP synthesis efficiency nor mitochondrial uncoupling

5   in the skeletal muscles of cachectic animals was shown to be altered [31], the compensatory

6   energy transduction was increased in the presence of dysregulation of glucose metabolism. In

7   this instance, the adipose tissue was broken down to catabolize circulating triacylglycerol.

8   Lipolysis not only regulates the homeostasis of systemic energy production but also leads

9   directly to the loss of adipose tissue. Recent studies in animal models of cachexia and in

10   humans have confirmed that the lipolysis of triacylglycerol is the primarily factor contributing

11   to fat loss [32]. Triacylglycerol is catalyzed to release fatty acids and to generate quantities of

12   acetyl-CoA, which overwhelms the transfer ability of carnitine acyltransferase. Subsequently,

13   ketone biosynthesis is enhanced, yielding 3-hydroxybutyrate and acetoacetate. Reports have

14   shown that skeletal muscle maintains increased usage of 3-hydroxybutyrate and lactate [33],

15   indicating that in cachexia, ketone bodies can be utilized as metabolic fuel for energy

16   metabolism.

17   Additionally, the most impacted pathway of muscle wasting was the biosynthesis of BCAAs,

18   accompanied by a gradual reduction in the valine, leucine, and isoleucine concentrations in

19   both the serum and the gastrocnemius muscle. Consistent evidence has shown that BCAAs

20   not only are an important energy substrate [34, 35], but they also act as precursors to improve

21   nitrogen retention and protein synthesis [36, 37]. Research has shown that leucine can stimulate

22   muscle protein anabolism [11], inhibit catabolism [38], and modulate glucose homeostasis [34]. The

23   infusion of leucine can promote the synthesis of glutamine and alanine, which are then

24   exported to the liver and are metabolized into glucose. Moreover, BCAAs are primarily

25   catabolized in the skeletal muscle; therefore, they are proposed for the treatment of catabolic

26   disease states.

27   Interestingly, the aromatic amino acid phenylalanine steadily increased in the serum. High

28   levels of phenylalanine can interfere with the production of serotonin and other amino acids,

29   as well as nitric oxide, which thus indicates metabolic reprogramming in cancer cachexia [22].

30   In a low-calorie environment, to maintain homeostasis, large amounts of neutral amino acids

31   are released and metabolized as an alternative energy-generating pathway. This process results

32   in high circulating concentrations of glutamine and aspartate. High levels of neutral amino

33   acids have been reported to promote an anabolic state by inhibiting proteolysis and directly

34   stimulating protein synthesis [39]. High protein turnover wastes the essential amino acids, which

35   cannot be supplied during cachexia. In the presence of amino acid hypermetabolism and

1   accelerated protein catabolism, amino acid intermediates, such as 3-methylhistidine and

2   creatine, were also found to be elevated in our study.

3   3-methylhistidine showed specificity for the indication of the wasting of muscle protein.

4   When actin and myosin are synthesized, histidine residues are methylated to construct the

5   cytocontractile apparatus in skeletal muscle fibers. However, during myofibrillar breakdown,

6   3-methylhistidines are released, and they cannot be recycled for intermediary metabolism or

7   protein synthesis. Based on its biology, serum or urine 3-methylhistidine represents gross

8   protein degradation and serves as a valuable biomarker for monitoring myofibrillar protein

9   degradation [40, 41]. Moreover, elevation of 3-methylhistidine could be detected before the

10 symptom of muscle wasting, suggesting the presence of increased muscle protein catabolism.

11 Creatine was another elevated amino acid intermediate found in the wasting muscle. Creatine

12 is produced by arginine, glycine, and methionine in the kidneys and liver. After being

13 transported into the blood, creatine is mainly taken up by the skeletal muscle through an

14 active transport system [42]. In fact, a large proportion of the total body creatine is distributed in

15 the skeletal muscle and is stored as phosphocreatine. In the state of catabolic

16 hypermetabolism and disrupted muscle metabolism, large pools of creatine circulate in the

17 blood. Therefore, the accumulation of serum creatine and excessive activated creatine kinase

18 are both markers for dysregulated muscle function [43].

19 In conclusion, the present study reports an integrated metabonomics analysis of serum and

20 intact gastrocnemius muscles from mice with cancer cachexia. Five distinguishable metabolic

21 features of cachexia were identified: low blood glucose, elevated ketone bodies, decreased

22 BCAAs, increased neutral amino acids and high amino acid intermediates. The consistent

23 metabolic profiles of serum and intact muscle imply a feasible and practicable diagnostic

24 approach for predicting skeletal muscle loss or other features of at-risk clinical populations

25 through the detection of serum metabolites. Moreover, the altered pathways could reveal the

26 potential metabolic mechanism of cancer cachexia.

27 Nevertheless, limitations must be considered in the present research. First, the complex

28 metabolic syndrome of cancer cachexia cannot currently be distinguished by a single

29 biomarker; however, the comprehensive evaluation of the five features is indicated as a

30 potential biomarker for the early detection of cancer cachexia. Second, all of the results were

31 acquired using the classic cancer cachexia model. Although further clinical studies are needed

32 to confirm the results, this dynamic model allowed us to directly identify metabolic profile of

33 intact muscle in a dynamic manner.

34

35

1   **Conflict of Interest**: The authors declare that they have no conflicts of interest.

2

6

7

References

1. K. Fearon, F. Strasser, S. D. Anker, I. Bosaeus, E. Bruera, R. L. Fainsinger, A. Jatoi, C. Loprinzi, N. MacDonald and G. Mantovani, *The lancet oncology*, 2011, **12**, 489-495.

2. K. Kalantar-Zadeh, C. Rhee, J. J. Sim, P. Stenvinkel, S. D. Anker and C. P. Kovesdy, *Journal of cachexia, sarcopenia and muscle*, 2013, **4**, 89-94.

3. K. C. Fearon, *New England Journal of Medicine*, 2011, **365**, 565-567.

4. J. A. Langius, S. Bakker, D. H. Rietveld, H. M. Kruizenga, J. A. Langendijk, P. J. Weijs and C. R. Leemans, *British journal of cancer*, 2013, **109**, 1093-1099.

5. S. Dodson, V. E. Baracos, A. Jatoi, W. J. Evans, D. Cella, J. T. Dalton and M. S. Steiner, *Annual review of medicine*, 2011, **62**, 265-279.

6. X. Zhou, J. L. Wang, J. Lu, Y. Song, K. S. Kwak, Q. Jiao, R. Rosenfeld, Q. Chen, T. Boone, W. S. Simonet, D. L. Lacey, A. L. Goldberg and H. Q. Han, *Cell*, 2010, **142**, 531-543.

7. I. Bosaeus, *Supportive care in cancer : official journal of the Multinational Association of Supportive Care in Cancer*, 2008, **16**, 447-451.

8. L. Santarpia, F. Contaldo and F. Pasanisi, *Journal of cachexia, sarcopenia and muscle*, 2011, **2**, 27-35.

9. M. J. Tisdale, *The journal of supportive oncology*, 2005, **3**, 209-217.

10. V. E. Baracos, *Cancer*, 2001, **92**, 1669-1677.

11. K. Fearon, J. Arends and V. Baracos, *Nature reviews. Clinical oncology*, 2013, **10**, 90-99.

12. V. E. Baracos, *Nutrition*, 2000, **16**, 1015-1018.

13. H. Der-Torossian, S. Asher, J. Winnike, A. Wysong, X. Yin, M. Willis, T.   O'Connell and M. Couch, *Metabolomics : Official journal of the Metabolomic Society*, 2013, **9**, 730-739.

14. T. M. O'Connell, F. Ardeshirpour, S. A. Asher, J. H. Winnike, X. Yin, J. George, D. C. Guttridge, W. He, A. Wysong and M. S. Willis, *Metabolomics*, 2008, **4**, 216-225.

15. Y. Quanjun, Y. Genjin, W. Lili, L. Bin, L. Jin, Y. Qi, L. Yan, H. Yonglong, G. Cheng and Z. Junping, *Molecular bioSystems*, 2013, **9**, 3015-3025.

16. W. E. Wang, D. Yang, L. Li, W. Wang, Y. Peng, C. Chen, P. Chen, X. Xia, H. Wang, J. Jiang, Q. Liao, Y. Li, G. Xie, H. Huang, Y. Guo, L. Ye, D. D. Duan, X. Chen, S. R. Houser and C. Zeng, *Circulation research*, 2013, **113**, 288-300.

17. Y. Tanaka, H. Eda, T. Tanaka, T. Udagawa, T. Ishikawa, I. Horii, H. Ishitsuka, T. Kataoka and T. Taguchi, *Cancer research*, 1990, **50**, 2290-2295.

18. O. Beckonert, H. C. Keun, T. M. Ebbels, J. Bundy, E. Holmes, J. C. Lindon and J. K. Nicholson, *Nature protocols*, 2007, **2**, 2692-2703.

19. N. Ebner, L. Steinbeck, W. Doehner, S. D. Anker and S. von Haehling, *Journal of cachexia, sarcopenia and muscle*, 2014, **5**, 27-34.

20. G. Zhang, B. Jin and Y. P. Li, *The EMBO journal*, 2011, **30**, 4323-4335.

21. M. Lima, S. Sato, R. T. Enos, J. W. Baynes and J. A. Carson, *Journal of applied physiology*, 2013, **114**, 824-828.

22. B. K. Ubhi, J. H. Riley, P. A. Shaw, D. A. Lomas, R. Tal-Singer, W. MacNee, J. L. Griffin and S. C. Connor, *The European respiratory journal : official journal of the European Society for Clinical Respiratory Physiology*, 2012, **40**, 345-355.

23. H. Norrelund, H. Wiggers, M. Halbirk, J. Frystyk, A. Flyvbjerg, H. E. Botker, O. Schmitz, J. O. Jorgensen, J. S. Christiansen and N. Moller, *Journal of internal medicine*, 2006, **260**, 11-21.

24. V. E. Baracos, *Journal of cachexia, sarcopenia and muscle*, 2011, **2**, 71-73.

25. R. P. Sah, S. J. Nagpal, D. Mukhopadhyay and S. T. Chari, *Nature reviews. Gastroenterology & hepatology*, 2013, **10**, 423-433.

26. T. Agustsson, P. Wikrantz, M. Ryden, T. Brismar and B. Isaksson, *Nutrition*, 2012, **28**, 851-855.

27. J. Z. Hu, *Methods in molecular biology*, 2011, **708**, 335-364.

28. O. Beckonert, M. Coen, H. C. Keun, Y. Wang, T. M. Ebbels, E. Holmes, J. C. Lindon and J. K. Nicholson, *Nature protocols*, 2010, **5**, 1019-1032.

29. G. P. Bongaerts, H. K. van Halteren, C. A. Verhagen and D. J. Wagener, *Medical hypotheses*, 2006, **67**, 1213-1222.

30. J. A. Tayek, *Journal of the American College of Nutrition*, 1992, **11**, 445-456.

31. C. M. Julienne, J. F. Dumas, C. Goupille, M. Pinault, C. Berri, A. Collin, S. Tesseraud, C. Couet and S. Servais, *Journal of cachexia, sarcopenia and muscle*, 2012, **3**, 265-275.

32. M. Lafontan, C. Moro, C. Sengenes, J. Galitzky, F. Crampes and M. Berlan, *Arteriosclerosis, thrombosis, and vascular biology*, 2005, **25**, 2032-2042.

33. H. D. Mulligan and M. J. Tisdale, *The Biochemical journal*, 1991, **277 (Pt 2)**, 321-326.

34. S. H. Adams, *Advances in nutrition*, 2011, **2**, 445-456.

35. V. E. Baracos and M. L. Mackenzie, *The Journal of nutrition*, 2006, **136**, 237S-242S.

36. P. L. de Campos-Ferraz, I. Andrade, W. das Neves, I. Hangai, C. R. Alves and A. H. Lancha, Jr., *Journal of cachexia, sarcopenia and muscle*, 2014, **5**, 105-110.

37. W. L. Morrison, J. N. Gibson and M. J. Rennie, *European journal of clinical investigation*, 1988, **18**, 648-654.

38. Z. Aversa, A. Bonetto, P. Costelli, V. G. Minero, F. Penna, F. M. Baccino, S. Lucia, F. Rossi Fanelli and M. Muscaritoli, *International journal of oncology*, 2011, **38**, 713-720.

39. G. Wu, *Amino acids*, 2009, **37**, 1-17.

40. M. Sheffield-Moore, E. L. Dillon, K. M. Randolph, S. L. Casperson, G. R. White, K. Jennings, J. Rathmacher, S. Schuette, M. Janghorbani, R. J. Urban, V. Hoang, M. Willis and W. J. Durham, *Journal of cachexia, sarcopenia and muscle*, 2014, **5**, 19-25.

41. N. Aranibar, J. D. Vassallo, J. Rathmacher, S. Stryker, Y. Zhang, J. Dai, E. B. Janovitz, D. Robertson, M. Reily, L. Lowe-Krentz and L. Lehman-McKeeman, *Analytical biochemistry*, 2011, **410**, 84-91.

42. S. A. Stimpson, S. M. Turner, L. G. Clifton, J. C. Poole, H. A. Mohammed, T. W. Shearer, G. M. Waitt, L. L. Hagerty, K. S. Remlinger, M. K. Hellerstein and W. J. Evans, *Journal of applied physiology*, 2012, **112**, 1940-1948.

43. S. S. Patel, M. Z. Molnar, J. A. Tayek, J. H. Ix, N. Noori, D. Benner, S. Heymsfield, J. D. Kopple, C. P. Kovesdy and K. Kalantar-Zadeh, *Journal of cachexia, sarcopenia and muscle*, 2013, **4**, 19-29.

1   **Figure Legends,**

2   Fig. 1. Line charts showing changes in carcass weight (A), dry carcass weight, (B) C26 colon

3   carcinoma size (C), the intact gastrocnemius muscle (D), and the protein expression of

4   MuRF1 (E) and MHC (F). The carcass weight decreased significantly from day 15 following

5   the implantation of the tumor. The dry carcass weight decreased relative to the wet carcass.

6   Moreover, the gastrocnemius muscle also showed a wasting trend that was related to the

7   expression of MHC.

8   Fig. 2. The typical 1H-NMR spectra of the serum from the dynamic cachexia mouse model.

9   The metabolites are assigned and marked. The overlapping peaks were identified by adding a

10   reference substance to the sample.

11   Fig. 3. The PLS-DA scores plot of the eight groups, based on the serum NMR spectra. G1-G7

12   represent the groups from day 9 to day 21 (every other day), and G8 is the control group. The

13   control group (G8) was separated from the tumor-bearing mice (G1-G7), and the

14   non-cachexia mice (G1-G2) were distributed over a time period different from the cachexia

15   period (G5-G7). The development of severe cachexia occurred over a dynamic track.

16   Fig. 4. The normalized concentration of the examined serum metabolites from non-cachexia

17   to severe cachexia. G1-G7 represent the groups from day 9 to day 21 (every other day).

18   Fig. 5. The typical HR-MAS NMR spectra of the intact gastrocnemius muscle tissue from the

19   dynamic cachexia mouse model. Unlike the metabolic profiles of the serum, the intact tissue

20   contained high levels of creatine and taurine and low glucose levels.

21   Fig. 6. The normalized concentration of the examined muscle metabolites from non-cachexia

22   to severe cachexia. M1 to M4 represent the groups from day 9 to day 21 (every three days),

23   and M0 is the control group.

24   Fig. 7. Cancer cachexia trigger the metabolic pathway reprogramming. The X axis represent

25   pathway impact, and the Y axis represent the $-\log(p)$. Biosynthesis of BCAA was the most

26   important impact pathway and $-\log(p) > 1.3$ was the statistically significant different pathways.

1   Table 1. The body characteristics of tumor-bearing mice from procachexia to the refractory cachexia period

	D9	D11	D13	D15	D17	D19	D21	Control
Heart (mg)	126.33±15.40	107.67±4.03[*]	127.5±26.01	112.50±20.73[*]	116.33±20.35[*]	102.83±33.08[*]	110.67±22.62[*]	124.00±25.49
Lung (mg)	138.17±12.53[*]	139.17±13.76[*]	141±13.64[*]	145.51±12.39[*]	143.01±17.13[*]	143.5±12.23[*]	131.17±11.09[*]	117.67±9.97
Liver (mg)	1225±81.99[*]	1226.5±70.53[*]	1351±60.97[*]	1332±182.71[*]	1303.5±416.04[*]	1256.67±199.52[*]	1221.5±231.6[*]	869.33±55.44
Spleen (mg)	131.67±19.48[*]	157.50±29.95[*]	215.83±21.67[*]	220.67±27.43[*]	286.67±43.26[*]	284.00±71.88[*]	210.83±114.83[*]	80.33±13.95
Kidney (mg)	364.5±28.33[*]	348.83±20.41[*]	353.33±34.85[*]	345.62±64.24[*]	338.33±24.96[*]	314.00±27.73	313.83±40.67	306.83±26.72
Gastrocnemius muscle (mg)	233.83±11.48[*]	228.00±15.13[*]	248±24.75[*]	227.00±16.75[*]	195.67±49.56[*]	213.17±18.86[*]	183.17±21.55[*]	322.67±119.41
Anterior tibial muscle (mg)	77.51±6.09[*]	86.33±16.51[*]	72.5±35.39[*]	80.67±14.88[*]	99.67±68.45[*]	62.50±32.10[*]	60.17±5.91[*]	112.01±34.39
Epididymis adipose (mg)	466.5±79.32[*]	412.17±51.94[*]	432.17±60.14[*]	328.21±67.11[*]	199.52±92.57[*]	137.67±105.16[*]		560.67±108.28
Tumor weight (mg)	476±331.78	864.17±473.13	2853.67±1060.09	3631.17±701.68	5130.07±0.94	7811.24±1.14	9522.41±0.84	
Carcass (g)	14.83±0.46	14.68±0.31	14.38±0.63	13.45±0.86[*]	12.75±1.25[*]	12.65±0.5[*]	11.83±1.59[*]	15.63±0.62
Dry body weight (g)	5.40±0.29	4.88±0.16[*]	4.82±0.27[*]	4.42±0.55[*]	4.37±0.36[*]	3.93±0.29[*]	3.47±0.42[*]	5.61±0.21

2   The data are shown as the mean ± SD. D9, D11 and so on are the days after tumor implantation. Each group included 6 mice, with the exception of 8 mice in
3   the control group. The control mice were sacrificed on day 7, which corresponded to the model animals. Values that were significantly different from the
4   control group (indicated by [*] $p < 0.05$) were determined by Tukey's post hoc test followed by one-way ANOVA.

420x320mm (96 x 96 DPI)
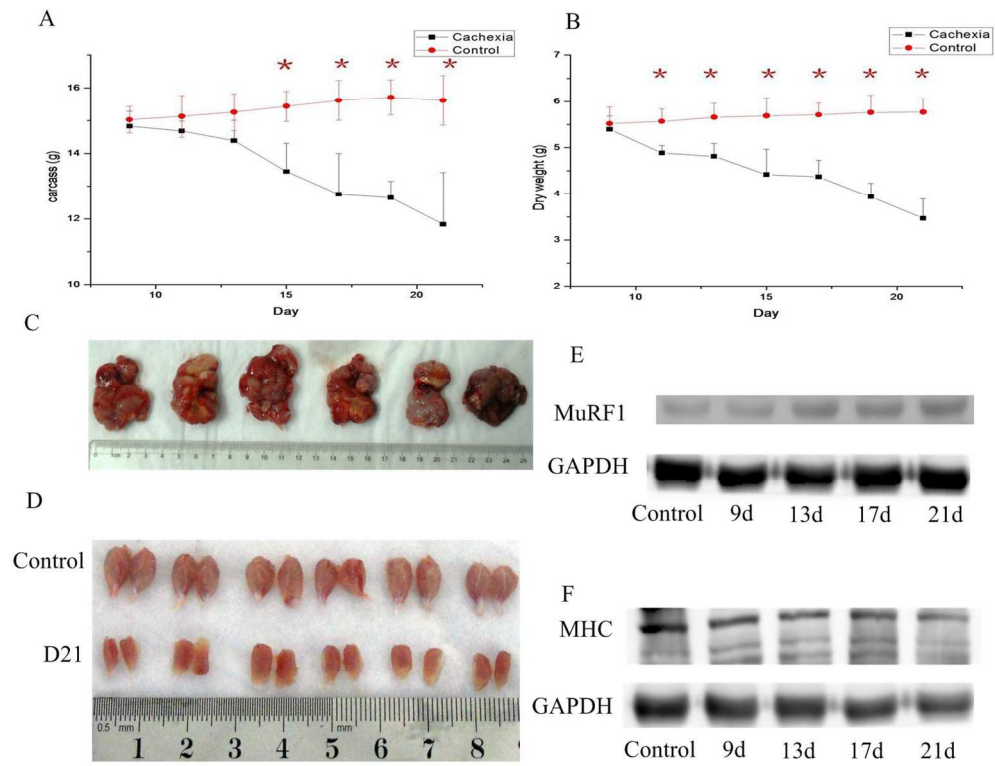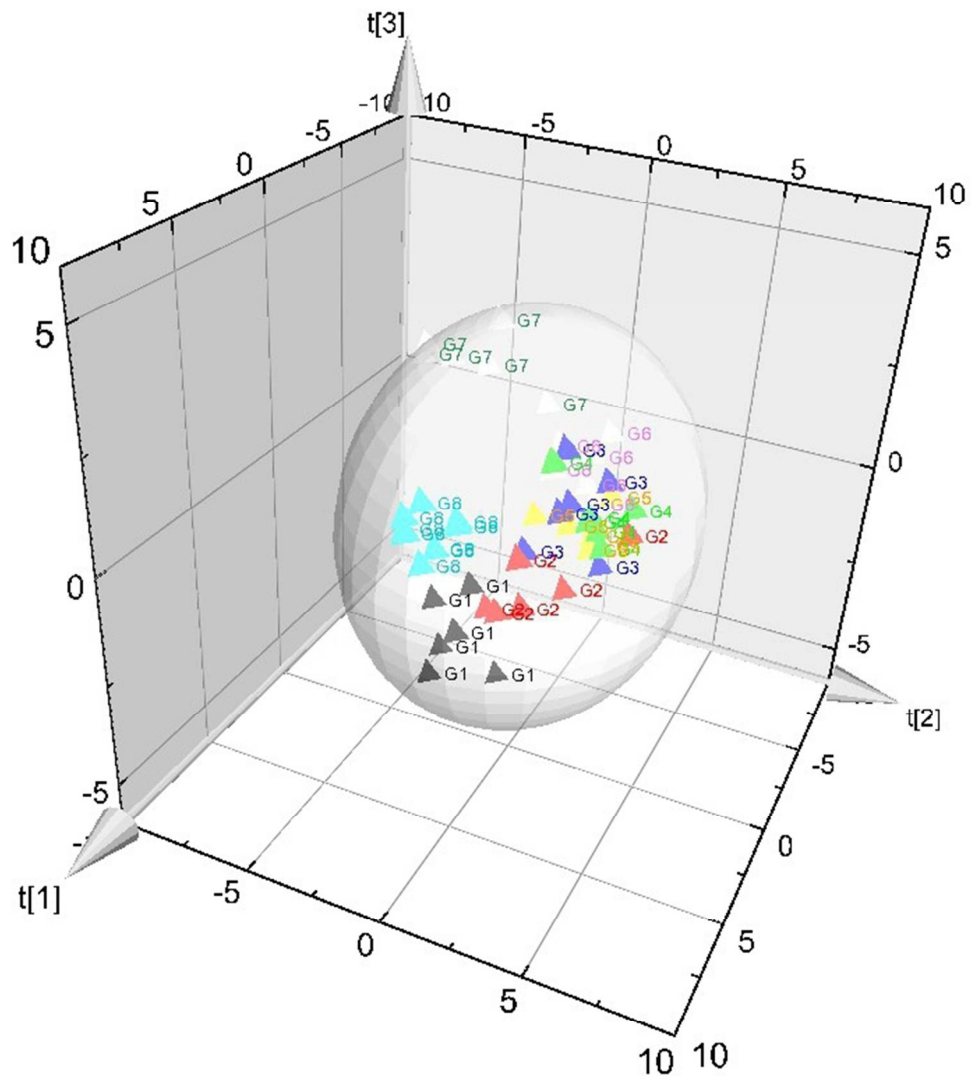
R2X[1] = 0.315228 R2X[2] = 0.207517 R2X[3] = 0.110247

189x213mm (96 x 96 DPI)
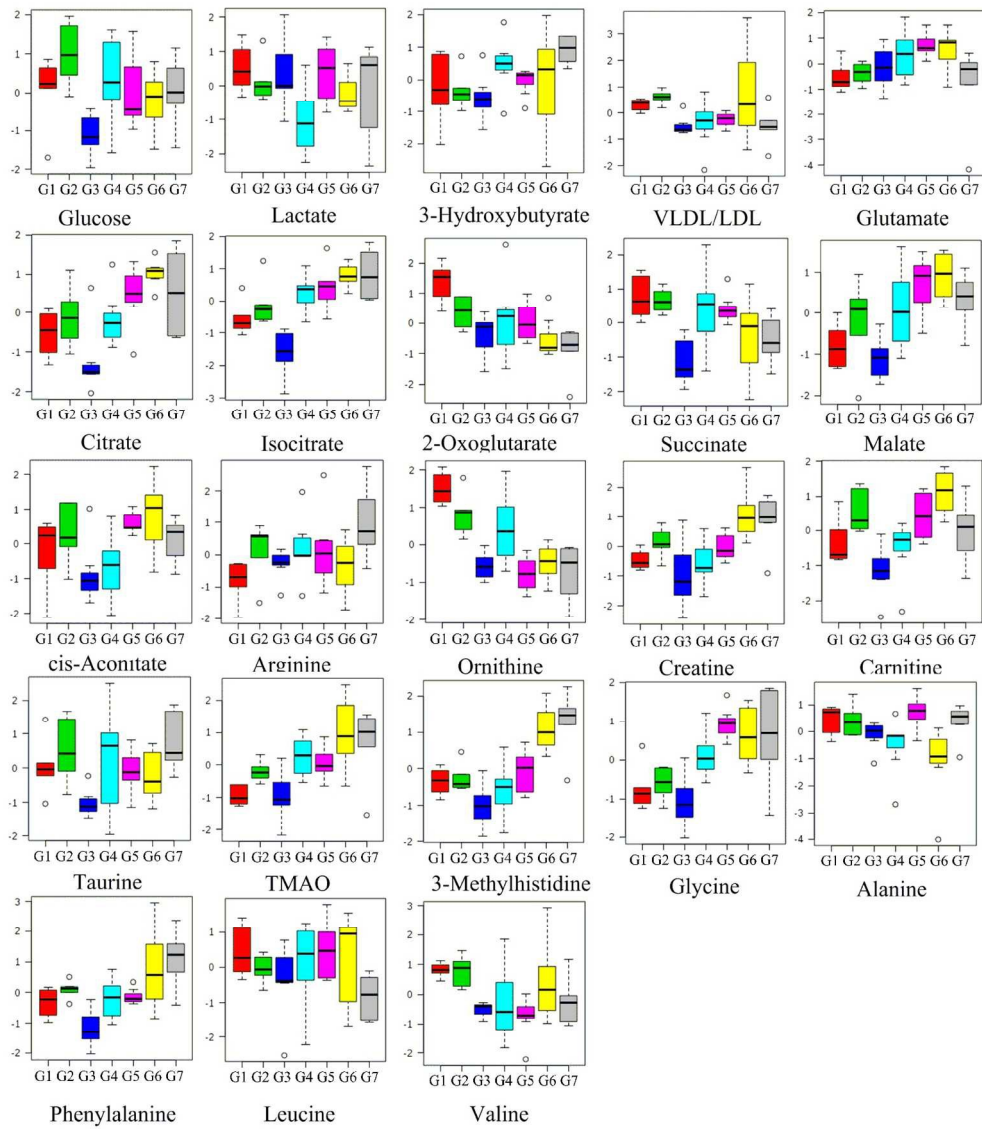
595x673mm (72 x 72 DPI)
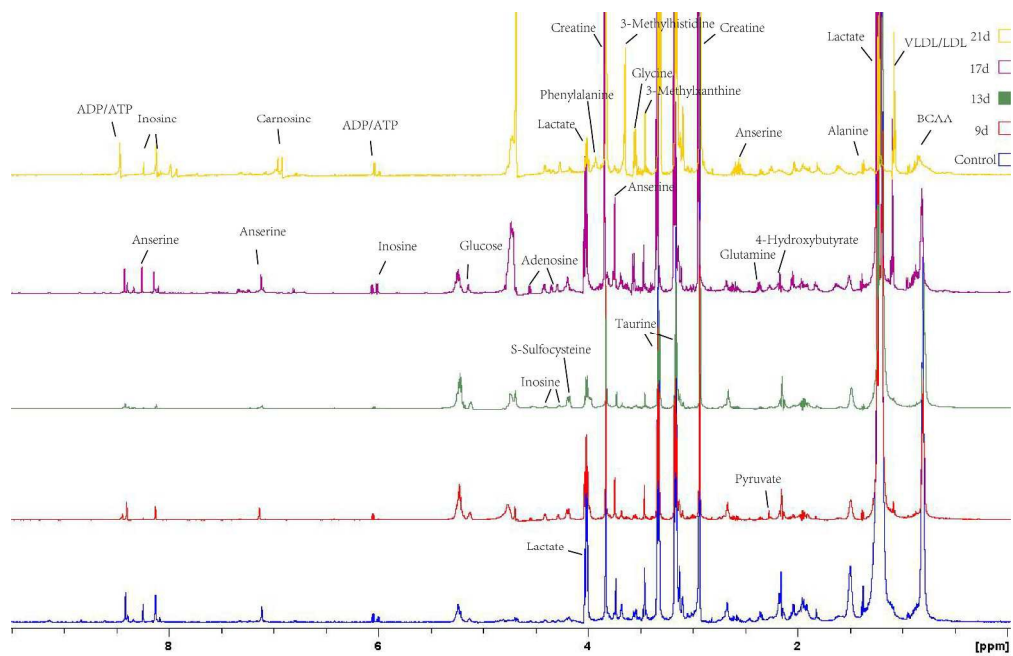
312x200mm (300 x 300 DPI)
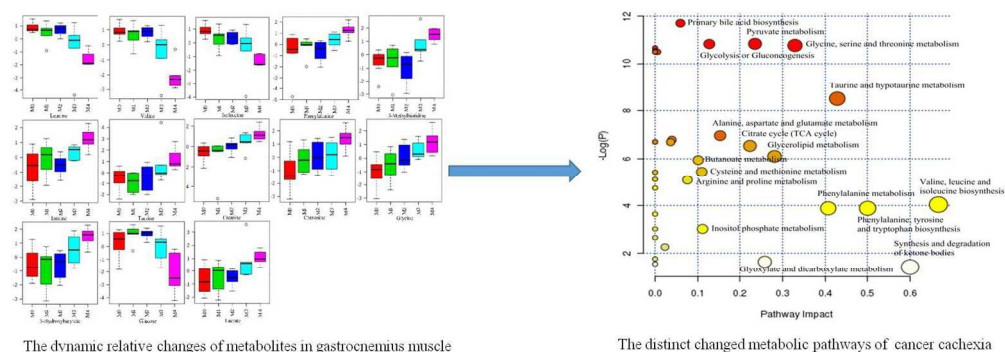
The dynamic relative changes of metabolites in gastrocnemius muscle

The distinct changed metabolic pathways of cancer cachexia

A dynamic murine cachexia model was established, and the serum was measured by solution NMR, as well as intact muscle measured by solid -state magic angle spinning NMR.
Forty-three metabolites were altered significantly in the serum and thirteen metabolites were altered in the muscle gastrocnemius.
Integrated analysis of dynamic metabolic profiles of serum and intact muscle reveal five distinct metabolic features of cancer cachexia, including low blood glucose, high ketone bodies, decreased branched-chain amino acids, increased neutral amino acids, and elevated amino acid intermediates.
278x102mm (150 x 150 DPI)
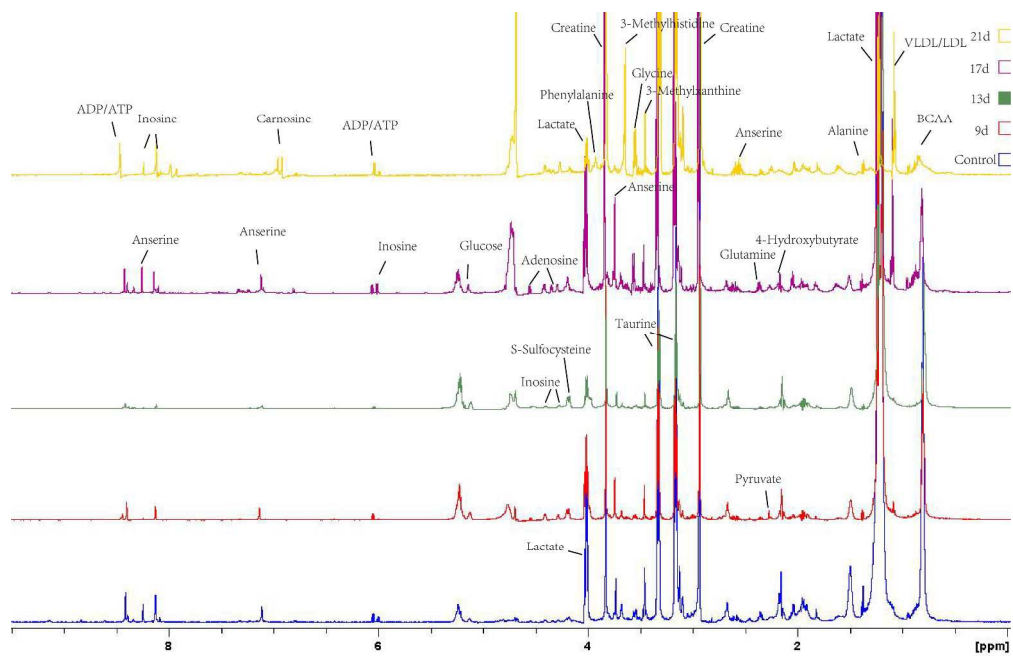
312x200mm (300 x 300 DPI)
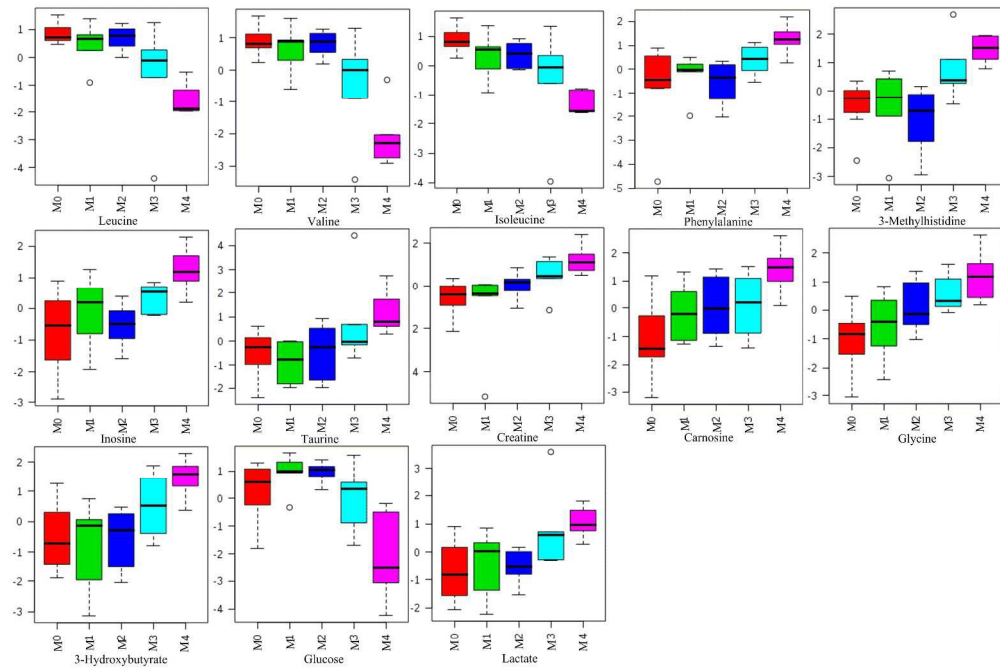
348x232mm (300 x 300 DPI)

260x249mm (300 x 300 DPI)